This is a preprint, the final version is subject to change, of the American Mineralogist (MSA)
Cite as Authors (Year) Title. American Mineralogist, in press.
(DOI will not work until issue is live.) DOI: http://dx.doi.org/10.2138/am-2015-5208

REVISION 1 - #5208, 12/23/14

Normal to inverse transition in martian spinel: Understanding the interplay between chromium, vanadium, and iron valence state partitioning through a crystal-chemical lens

James J. Papike[1], Paul V. Burger[1], Aaron S. Bell[1], Charles, K. Shearer[1], Loan Le[2], and John Jones[3]

[1]Institute of Meteoritics, Department of Earth and Planetary Sciences, University of New Mexico, Albuquerque, New Mexico 87131, U.S.A., [2]JSC Engineering, Technology and Science (JETS), NASA Johnson Space Center, Houston, Texas 77058, U.S.A., [3]NASA Johnson Space Center, Houston, Texas 77058, U.S.A.

Submitted to American Mineralogist, "Outlook Paper" Centennial Volume

ABSTRACT

Spinel is a very important rock-forming mineral that is found in basalts from Earth, Mars, the Earth's Moon, and basaltic meteorites. Spinel can be used as a sensitive indicator of petrologic and geochemical processes that occur in its host rock. This paper highlights the role of increasing fO_2 (from IW-1 to FMQ+2) in converting a >90% normal spinel to an ~25% magnetite (inverse) spinel, the trajectory of $D_V^{spinel/melt}$ as it relates to the ratio of V^{3+}/V^{4+} in the melt, and the crystal chemical attributes of the spinel that control the intrinsic compatibility of both V^{3+} and V^{4+}. This work examines the nuances of the V partitioning and provides a crystal chemical basis for understanding Fe^{3+}, Cr, and V substitution into the octahedral sites of spinel. Understanding this interplay is critical for using spinels as both indicators of planetary parentage and reconstructing the redox history of magmatic systems on the terrestrial planets. Three

potential examples for this use are provided. In addition this work helps explain the ubiquitous miscibility gap between spinels with changing ülvospinel contents.

INTRODUCTION

Spinels are a common accessory phase in many terrestrial and extraterrestrial materials and their structure and composition are uniquely responsive to changing conditions (e.g. Haggerty 1972, 1976; Lindsley 1976, 1991; Basaltic Volcanism Study Project 1981; McKay et al. 2004a,b; Righter et al. 2006; Ishizawa et al. 2014). Specifically, the spinel structure and its inherent ability to accommodate multi-valent cations such as V, Cr, and Fe is highly sensitive to changing temperature and fO_2 conditions (e.g. Hill and Roeder 1974, McKay et al. 2004a,b; Muan et al. 1972, Righter et al. 2006).

Papike et al. (2004) suggested that zoned, magmatic spinels could be used to determine relative oxygen fugacities and planetary parentage. This study specifically noted that the behavior of V is very different when comparing terrestrial, lunar, and martian basalts. In terrestrial basaltic liquids, typically $V^{4+} > V^{3+}$, whereas in lunar basalts $V^{3+} > V^{4+}$, and in martian basalts V^{3+} and V^{4+} are both significant. The core to rim trends for lunar spinels show a strong positive correlation of V and Cr and negative correlation of V and Ti. For the Earth, the trends are just the opposite, with a strong negative correlation of V and Cr and strong positive correlation of V and Ti. Chromite in martian basalts shows intermediate trends. These systematics suggest that at high oxygen fugacity (Earth), V^{4+} follows Ti^{4+}, whereas at low oxygen fugacity (Moon), V^{3+} follows Cr^{3+}.

These qualitative interpretations of vanadium behavior were subsequently investigated using a series of experiments to better understand the potential of V behavior in spinels as an oxybarometer (e.g. Papike et al. 2004, 2005, 2013, 2014). The experiments illustrated the

relationships between Fe^{2+}-Fe^{3+} and V^{3+}-V^{4+}, in which the vanadium in spinel, V^{3+} is best incorporated in normal spinel as $^{IV}Fe^{2+VI}V^{3+}{}_2O_4$ (coulsonite) and V^{4+} as $^{IV}Fe^{2+VI}(Fe^{2+}V^{4+})O_4$ (synthetic compound, inverse spinel) (Rodgers et al. 1963).

The intent of this study is to explore the relationships between V partitioning behavior and spinel crystal chemistry at magmatic conditions over several orders of magnitude in fO_2. In particular, we examine (1) the interplay among normal-inverse spinel structure, Fe^{2+}-Fe^{3+}, and V partitioning and (2) the importance of using this interaction for interpreting petrologic conditions for the origin of extraterrestrial materials.

CRYSTAL CHEMISTRY OF SPINEL

The potential interplay between vanadium and iron valance states in the context of the spinel crystal chemistry is partially illustrated in Figure 1. This figure shows the crystal structure of both normal and inverse spinel. The normal spinel structure (Fig. 1a) is represented by magnesiocoulsonite, $^{IV}Mg^{VI}V^{3+}{}_2O_4$ (see Papike et al. 2005 and references therein). In naturally occurring normal spinel, the sixteen octahedral sites per unit cell (Papike et al. 2005) are occupied by trivalent cations Cr, Al, V^{3+}, etc., while the eight tetrahedral sites per unit cell are occupied mainly by Mg and Fe^{2+}. The inverse spinel structure (Fig. 1b) is represented by magnetite, $^{IV}Fe^{3+\ VI}(Fe^{2+}Fe^{3+})O_4$. In naturally occurring inverse spinel, the sixteen octahedral sites per unit cell are occupied by tetravalent, trivalent, and divalent cations, Ti^{4+}, Fe^{3+}, Cr^{3+}, Al^{3+}, V^{3+}, Fe^{2+}, while the eight tetrahedral sites per unit cell are occupied mainly by cations such as Fe^{3+}. In Figure 1c, synthetic inverse vanadium spinel is represented by $^{IV}Fe^{2+\ VI}(Fe^{2+}V^{4+})O_4$ (Rodgers et al. 1963). This spinel is referred to as V-inverse in this paper. This synthetic compound has the same structure as ulvöspinel, with V^{4+} taking the place of Ti^{4+}. In a study by Wechsler et al. (1984), the authors point out that (based on neutron diffraction), all Ti is confined

to the sixteen octahedral sites per unit cell, none enters the eight tetrahedral sites. We assume that the same holds true in our own experiments. Thus even in spinel at reducing conditions such as IW-1, which is largely chromite with the normal spinel structure $^{IV}(Mg, Fe^{2+})^{VI}Cr^{3+}{}_2O_4$, small domains of the inverse structure must exist in order to accommodate Ti.

Spinels with chromite contents between 0.00 and 0.48 mole fraction are characterized by domains that are dominantly "normal" spinel, while those with ülvospinel contents greater than 0.88 mole fraction ülvospinel contain domains that are dominantly "inverse." See Haggerty (1972) for documentation of this miscibility gap. The result is that the lowest free energy assemblage is a two-phase region of a chromite-rich spinel and an ülvospinel-rich spinel coexisting across a miscibility gap. This explains the ubiquitous miscibility gap between spinels with ülvospinel contents less than 0.48 mole fraction ülvospinel/(ülvospinel + chromite) and those with greater than 0.88 mole fraction ülvospinel.

EXPERIMENTAL AND ANALYTICAL APPROACHES

Experiments

All of the Yamato 980459 (Y98) composition partitioning experiments were conducted in the gas mixing laboratory at NASA Johnson Space Center. The majority of the experiments were performed using Re wire loops to prevent Fe-loss. Experiments run at oxygen fugacities at or above the FMQ buffer employed Pt/Rh-alloy wire loops. Experimental fO_2 was controlled using CO/CO_2 gas mixtures that were calibrated with a Y-stabilized zirconia electrochemical oxygen sensor, specifically the SIRO2 from COF-Australia, housed in a dedicated reference furnace. Experiments were conducted at discrete fO_2 intervals separated by approximately 1 log unit. The experimental fO_2 values ranged from ΔIW-1 to ΔIW+5.4. Experiments were conducted with an initial, eight hour super-liquidus dwell at 1450˚C. At the end of the super-liquidus soak, the

93 temperature was dropped at 0.25˚C sec^{-1} until reaching the final target temperature of 1200˚C.
94 Experiments were terminated by drop quenching the charge into water. The synthetic Y98
95 composition used in the experiments was made from a mixture of synthetic oxide powders that
96 were fused to form a homogenous glass. This glass was milled to a fine-grained powder prior to
97 being used in the experiments. The composition of the glass was patterned after the reported
98 composition of the bulk Y98 meteorite. Additionally, starting glass was also doped with 0.20 wt.
99 % V_2O_3, EuO_2 and CeO_2.

100 **Electron microprobe (EPMA)**

101 Analyses were collected on the JEOL JXA 8200 electron microprobe at the Institute of
102 Meteoritics (IOM) and Department of Earth and Planetary Sciences (E&PS), at the University of
103 New Mexico (UNM). Backscattered electron imaging and analyses were collected at an
104 accelerating voltage of 15 kV. Oxide phases were analyzed using a probe current of 20 nA, and a
105 spot size of 0-2 μm. Glass analyses were collected at a beam current of 10 nA, and a spot size of
106 5 μm to limit beam volatilization. Elements were calibrated using C.M. Taylor Co. EPMA
107 standards, as well as additional standards developed in-house; a separate calibration was used for
108 the oxides and the glass. Vanadium measurements were made under typical analytical
109 conditions, i.e., 40 second peak counting and 20 seconds on both background positions. The Ti
110 interference on V was specifically determined for our spectrometer configuration (with the Ti Kβ
111 peak representing a known interference for V Kα), as was the Cr Kβ interference on Mn Kα.
112 Ferric iron in the spinel was calculated using the methodology of Droop (1987).

113 Uncertainties associated with the calculated partition coefficient values (e.g., for
114 $D_V^{spinel/glass}$) were propagated using the 1σ standard deviations and the mean of the EPMA
115 determined vanadium analyses. Typically, the 1σ standard deviation for a given population of

vanadium analyses was greater than the 2σ analytical uncertainty derived from x-ray counting statistics; therefore, we feel the use of the 1σ standard deviation is a more accurate portrayal of the actual uncertainties that arise from subtle compositional inhomogeneity.

RESULTS

Major and minor element chemistry of both spinel and glass are presented in Table 1. Analyses were collected in samples spanning the fO_2 range of IW-1 to FMQ+2. Analytical conditions were tailored to the phases being analyzed, and are discussed in detail in the experimental and analytical approach section above.

The major element chemistry of the spinels is generally defined by an increase in magnetite component at the expense of the chromite and spinel components with increasing fO_2. This can be seen in changes in the concentration of the elements that define those components. The average aluminum content of the spinels drops from 8.62 wt.% Al_2O_3 at IW-1 to 5.96 wt.% at FMQ; at FMQ+1 and FMQ+2, Al_2O_3 jumps up slightly to 7.30 and 6.95 wt.%, respectively. Chromium initially increases from 46.06 wt.% Cr_2O_3 at IW-1 to 54.87 wt.% at FMQ, but increasing fO_2 results in a drop in Cr_2O_3 to 39.83 and 40.42 wt.% at FMQ+1 and FMQ+2, respectively. The calculated Fe_2O_3 concentration increases from 0.94 wt.% to 8.12 wt.% at FMQ; increasing the fO_2 results in further increases in Fe_2O_3, where at FMQ+1 and FMQ+2, it was calculated to be 17.27 and 17.53 wt.%, respectively (Fig. 2a). Figure 2b shows the modeled Cr^{3+}/ total Cr in glass (discussed more below). Figure 2c illustrates measured vanadium in spinel, and Figure 2d presents modeled ferric iron in the liquid. All of these are discussed below. Vanadium concentration in spinel initially shows a decrease with increasing fO_2. The V_2O_3 concentration of the spinel drops from 9.16 wt.% to 1.58 wt.% in the IW-1 and FMQ experiments, respectively (Fig. 2c). Increasing fO_2 further results in a slight bump in V, to 2.40

and 2.22 wt.% V_2O_3, at FMQ+1 and FMQ+2, respectively. Remaining major and minor element chemistry in the spinels is detailed in Table 1.

Analyses collected in the glasses in the experiments indicate that Cr decreases in the melt with increasing fO_2, while V increases (Table 1). The Cr_2O_3 concentration varies from 0.37 wt.% in the IW-1 experiment to 0.12 wt.% in the FMQ+2 experiment. The V_2O_3 concentration increases from 0.20 wt.% in the IW-1 experiment, to a high of 0.33 wt.% in the FMQ+2 experiment. Partition coefficient values, calculated for V between spinel and melt ($D_V^{spinel/melt}$), generally drop from the low fO_2 experiments through the more oxidized samples (Fig. 3, Table 1). The calculated values range from 45.2 at IW-1, down to 6.2 at FMQ. The experiments at even higher fO_2 show some variability in the partition coefficient; $D_V^{spinel/melt}$ is calculated at 7.6 and 6.8 at FMQ+1 and FMQ+2, respectively.

DISCUSSION

The Effect of fO_2 on Spinel Composition and the Compatibility of V^{3+} and V^{4+}

Not only does fO_2 profoundly change the spinel-melt partitioning systematics of V, but it also exerts a significant influence on the valence ratios of Fe^{3+} to Fe^{2+} and Cr^{3+} to Cr^{2+} in the melt. The availabilities of Cr^{3+}, Fe^{2+}, and Fe^{3+} in the melt should, in some way, also be manifested in the equilibrium composition of the spinel. Changes in the major element composition of spinel have been indirectly observed to have important consequences for the compatibility of V in the spinel structure (Canil 2002; Righter et al. 2006 and Mallmann and O'Neill 2009). The underlying crystal chemical reasons for these effects are discussed in detail in the following section. In this section we focus the discussion on how changes in Cr and Fe valence influence both the composition and structure of the equilibrium spinels.

The spinel components have been plotted as a function of fO_2 in Figure 4. This figure clearly illustrates two important points: (1) the major element composition of the spinel is relatively constant as fO_2 is increased from IW-1 to IW+3.4 (i.e., FMQ), and (2) at fO_2 values >IW+3.4, the composition of the spinel shows a significant increase in its magnetite component accompanied by a reduction in the spinel and ferro-chromite components.

The availability of Cr^{3+} in the melt is an important parameter that plays a critical role in defining the stability field of spinel with respect to both its position on the liquidus, as well as its equilibrium composition, and therefore has important implications for V stability in spinel as well. Several recent studies have demonstrated the Cr^{3+}/Cr^{total} (Fig. 2b) in basaltic melts changes dramatically as fO_2 is increased from values near the IW buffer to values near the FMQ buffer (Hanson and Jones 1998; Berry et al. 2006 and Bell et al. 2014). Curiously, the increase in Cr^{3+}/Cr^{2+} of the melt does not appear to significantly increase the chromite content of the experimental spinels. Importantly, this observation suggests that fO_2 has only a minor effect on spinel composition in the fO_2 space where the concentration of ferric iron in the melt is minimal. The increase in the Cr^{3+}/Cr^{2+} ratio that accompanies the oxidation of the melt appears to be accommodated through the crystallization of additional Cr-rich spinel. This observation is corroborated by the monotonic decrease in the Cr^{total} content of the melt that occurs with increasing fO_2. In contrast, the effect of ferric iron on the composition of the spinel is relatively pronounced. The increasing abundance of Fe^{3+} in the melt results in the spinel being steadily enriched in the magnetite component and depleted in the $MgAl_2O_4$ component.

From a structural point of view, the observed change in spinel composition can be understood as follows: at low oxygen fugacity, ~IW-1 to IW+3, the structure is that of normal spinel, in which the sixteen octahedral sites per unit cell (Papike et al. 2005) are occupied by

trivalent cations, Cr, Al, V^{3+} etc., while the eight tetrahedral sites per unit cell are occupied mainly by Mg and Fe^{2+}. Spinel at IW-1 to IW+3 must be dominated by the normal spinel structure, only containing isolated domains of the inverse structure to accommodate elements such as Ti^{4+} and limited quantities of Fe^{3+}. However, in the oxygen fugacity range above IW+3, the increasing Fe_2O_3 in the melt causes a significant shift in the spinel composition, where domains of the inverse spinel structure (which have lower free energy than the normal spinel structure) become increasingly prevalent.

The observed changes in the spinel composition have important implications for the compatibility of V^{3+} and V^{4+} in the octahedral sites of the spinel. For example, V^{3+} is highly compatible in Cr-rich normal spinel as it can readily substitute for Cr^{3+}. Normal spinels have difficulty accommodating higher valence cations in the octahedral sites due to charge balance issues, therefore small, highly charged cations such as Ti^{4+} and V^{4+} only partition weakly into these sites. In contrast to this behavior, 4+ cations are much more compatible in the inverse spinel structure where divalent cations occupy the tetrahedral sites in order to maintain charge balance. The consequences of this change in spinel composition and structure will be explored in detail in the next section of the work.

The variation of $D_V^{spinel/glass}$ with Oxygen Fugacity

The observed trend in the vanadium partition coefficients (Fig. 3a) must be interpreted with respect to both the ratio of V^{3+} to V^{4+} in the melt, as well the changing major element composition and structure of the spinel. It is represented schematically in Figure 5. In an attempt to disentangle the crystal chemical effects on $D_V^{spinel/glass}$ from that of the changing V^{3+}/V^{4+} in the melt, we have modeled the $D_V^{spinel/glass}$ as a function of fO_2 for the experimental spinels (Fig. 3b). It is clear from this figure that increasing fO_2 depresses the $D_V^{spinel/glass}$ value. The model

assumes that: 1) V^{3+} and V^{4+} are the two valence states present in the melt and 2) the $D_{V3+}^{spinel/melt}$ and $D_{V4+}^{spinel/melt}$ values are static (i.e., they are independent of the major element composition of the spinel and comply with Henry's Law). The total partition coefficient for vanadium can therefore be expressed as:

$$D_V^{spinel/melt} = (xV^{3+}_{melt} D^{V^{3+}}) + (xV^{4+}_{melt} D^{V^{4+}})$$

In the case of our experiments, the effects of fO_2 on the major element compositions of the experimental spinels are minimal at fO_2 values lower than IW+2. Therefore, the use of static D values in this fO_2 range is justified. However, calculating the $D_V^{spinel/melt\ (effective)}$ requires knowledge of the molar concentrations of V^{3+} and V^{4+} in the melt. Previous spectroscopic studies of V valence in silicate melts have convincingly demonstrated that V^{3+} comprises >80% of the total V in melts of basaltic compositions (Righter et al. 2006 and Sutton et al. 2005) at reduced conditions (i.e., fO_2 <IW). Through trial and error, we found that modeling the $D_V^{spinel/melt}$ curve using a V^{3+}/V^{total} value of 0.90 for the IW-1 experiment and $D_{V3+}^{spinel/melt} \sim 48$ and $D_{V4+}^{spinel/melt} = 3$ yielded the best match for the observed trend of our partitioning data.

This modeling also helps clarify the role of Fe^{3+} on the inverse component of the spinel. In the most oxidized experiments, the model curve shows a significant divergence from the measured $D_V^{spinel/melt}$ curve. The divergence of the model curve and measured $D_V^{spinel/melt}$ values can be explained by an increase in the compatibility of V^{4+} in the spinel structure (Papike et al. 2004, 2005), as it becomes more inverse. This change in structure is facilitated by the increasing concentration of Fe^{3+} in both the spinel (as magnetite) and the melt. Furthermore, the modeling clearly shows that in the spinels that contain little Fe^{3+} and have a constant Cr/Al, the $D_V^{spinel/melt}$

can be modeled as a simple function of the V^{3+}/V^{4+} present in the melt. This simplified approach, however, cannot be used for spinels that have a substantial portion of inverse domains. In the case of our experiments, the rise of the inverse structure coincides with rise of Fe^{3+} in the melt with increasing fO_2. Although not explicitly addressed by our experiments, this effect is also important for spinels enriched in the ülvospinel component.

Spinels as indicators of planetary parentage and redox histories

This manuscript illustrates the interplay among multivalent cations ($Fe^{2+,3+}$, $Cr^{2+,3+}$, $V^{3+,4+}$), the spinel structure, and oxygen fugacity in determining the partitioning behavior of vanadium. Understanding this interplay is critical for using spinels as both indicators of planetary parentage and reconstructing the redox history of magmatic systems on the terrestrial planets. Three examples for this use are given below.

Example 1. Papike et al. (2005) and Karner et al. (2003) illustrated the usefulness of silicates (olivine, pyroxene, and plagioclase) for determining planetary parentage of extraterrestrial materials. These approaches have been used in countless studies of meteorites (e.g. Fagan et al. 2002; Agee et al. 2013; Elardo et al. 2013). Papike et al. (2004, 2013) illustrated the qualitative usefulness in relating spinel chemistry to both a parent body source and the fO_2 of a planetary body mantle and its associated basalt systems. As discussed in those papers, differences in fO_2 among basaltic systems associated with the Earth's moon and primitive, differentiated small bodies such as the eucrite parent body (~IW-1), the Earth (FMQ±1), and Mars (IW+1 to FMQ) have profound implications for the valence state of multi-valent cations and the spinel structure. The planetary environments that are reduced will be dominated by normal spinels and the reduced species of multi-valent cations. More oxidizing environments, such as the Earth (FMQ±1), and Mars (IW+1 to FMQ), will be dominated by the

transition between normal and inverse spinels and the more oxidized species of multi-valence cations. These differences strongly influence partitioning behavior during mantle melting and subsequent crystallization, and thereby result in differences in spinel compositions.

Example 2. A prominent geochemical feature of the shergottites is the large range in initial Sr isotopic ratios (~0.702 – 0.724) and initial ε^{Nd} values (~ -10 to +50) (e.g., Nyquist et al. 2006; Borg et al. 2012; Brandon et al. 2012; Shearer et al. 2008; Symes et al. 2008). Within this range of isotopic characteristics, the shergottites also exhibit a systematic variation in the oxygen fugacity of crystallization (Wadhwa 2001; Herd 2006; Borg et al. 2003, 2005; Borg and Drake 2005; Shearer et al. 2008; Symes et al. 2008). To decipher the petrogenesis of the shergottites, a fuller understanding of the petrologic linkages between these geochemical characteristics and intensive parameters (fO_2) must be reached. One approach to deciphering these petrogenetic linkages is to examine the crystallization history preserved in spinel compositions of a single magma and compare the history preserved by spinel populations in different magmas.

Spinels in the shergottites exhibit substantial compositional differences among early spinels from different shergottites and along crystallization trajectories within individual shergottites (e.g. Goodrich et al. 2003; McKay et al. 2004a,b; Peslier et al. 2010; Gross et al. 2011). Early spinels in the isotopically depleted shergottites such as Y980459, NWA 5789, SaU 005, and Dhofar 019 have relatively low magnetite (1 to 2%) and inverse spinel components (magnetite + ülvospinel ~ 4 to 5%). Therefore, fO_2 estimates from V partitioning in these lithologies should be relatively unaffected by the presence of an inverse structural component. Comparison with our data suggests an fO_2 of crystallization for Y980459 of IW+1.

On the other hand, the more isotopically enriched shergottites such as NWA 1110 and EETA 79001 have early spinel with higher magnetite (3 to 6%) and inverse spinel components

(magnetite + ülvospinel ~ 5 to 7%). Based on comparison with our data, the fO_2 of crystallization for the enriched shergottites is more oxidizing than IW+2. All of the early spinels have similar chromite-ülvospinel-spinel components and overlapping V_2O_3. This suggests similar bulk $D_V^{spinel/melt}$ and slightly different bulk V in the magma. Examining the spinel crystallization trajectories, the magnetite and inverse spinel components increase only slightly, with the magnetite component increasing to 2-5% and the inverse spinel component increasing (magnetite + ülvospinel ~ 8 to 15%). Also, there is an overall increase in the V component in these spinels. Based on our results, this suggests only a subtle increase in fO_2 during crystallization.

In contrast, several of the depleted olivine-phyric shergottites exhibit a substantial increase in both the magnetite (13-15%) and the inverse spinel components (magnetite + ülvospinel ~ 18 to 20%). These data suggest that the fO_2 becomes increasingly oxidized during crystallization. Very little V data exists for these spinels, but based our analysis would predict an overall decrease in bulk $D_V^{spinel/melt}$ and therefore a decrease in the V content of the late spinels. These initial observations are only the beginning. Combining the experimental data and interpretations with a much more detailed analytical dataset of spinels from the shergottites would yield a much more profound understanding of the fO_2 record preserved in martian spinels.

Example 3. The differentiation of asteroids is one of the most fundamental processes to have occurred in the early Solar System. There are numerous families of achondrite meteorites that represent partial melting of these small parent bodies (e.g. eucrites, diogenites, acapulcoites, lodranites, brachinites, and unclassified Na-rich achondrites such as GRA 06129/06128). Several of these achondrites represent magmatism on parent bodies with a well-defined fO_2 (e.g. eucrites and diogenites ~ IW-1). Other achondrites are derived from parent bodies with fO_2 that are not well-defined (e.g. brachinites, unclassified Na-rich achondrites such as GRA 06129/06128). As

has been demonstrated, differences in the fO_2 (IW-1 to IW+2) during partial melting on these parent bodies will produce considerably different melt compositions (e.g. Jurewicz et al. 1995; Garder-Vandy et al. 2013; Usui et al. 2014). Several studies have linked brachinites to unique sodium feldspar-rich achondrite GRA 06129/06128 (e.g. Shearer et al. 2010; Usui et al. 2014). Usui et al. (2014) illustrated that partial melting of a chondritic precursor would yield a brachinite residuum and a GRA 06129 melt, under specific fO_2 conditions. As both lithologies contain Cr-spinels, examining the systematic relationship between their chemistries and fO_2 would allow for an analysis of conditions of melting and crystallization. The spinels in brachinites have a Cr/(Cr+Al) of 0.73 to 0.83. The extent of the magnetite component is debated, but is thought to be approximately 1 to 3%. Complicating the interpretation of this data is the subsolidus reequilibration experienced by both of these primitive lithologies.

This work demonstrates the nuances of the V partitioning and provides a crystal chemical basis for understanding Fe^{3+}, Cr, and V substitution into the octahedral sites of spinel. The above examples illustrate the importance of understanding this interplay for using spinels as both indicators of planetary parentage and reconstructing the redox history of magmatic systems on the terrestrial planets.

IMPLICATIONS

We seek to understand the origin and evolution of the solar system. There are many ways to do this: theory, experimental approaches and space missions with orbital and landed experiments. Arguably, the most powerful approach is to have a sample from the specific body we want to understand. In some cases this is not currently possible given the costs or the lack of critical technology to enable such missions (e.g., obtaining samples from Europa or the center of Jupiter). The book “Basaltic volcanism in the terrestrial planets” (Basaltic Volcanism Study

Project, 1981) was an early attempt to address the issue of understanding processes in the solar system as recorded by basalts. A team led by the first author (JJP) participated in this exciting study by pulling together information on the silicates from planetary basalts. In the present study we follow giants in the field (Haggerty 1976; Lindsley 1976, 1991; Basaltic Volcanism Study Project, 1981) including S.E. Haggerty (Haggerty 1976; his contribution to Basaltic Volcanism Study Project, 1981) who was a leader in the study of spinels. We hope our work, both preceding and specifically in this paper, will make the use of spinel chemistry, crystal chemistry, and valence state partitioning even more powerful.

The use of a single zoned spinel from (normal spinel, chromite) to (inverse spinel ülvospinel-magnetite) can, with use of the ratios of Fe^{2+}, Fe^{3+},Cr^{2+}, Cr^{3+}, $V^{2+,3+,4+,5+}$ compared to the other elements in the core to rim zoning trend of a single spinel crystal, identify the planetary parentage of the grain and (if the melt composition is known) the quantitative oxygen fugacity trajectory during crystallization of the host basalt.

REFERENCES CITED

Agee, C.B., Wilson, N.V., McCubbin, F.M., Ziegler, K., Polyak, V.J., Sharp, Z.D., Asmerom, Y., Nunn, M.H., Shaheen, R., Thiemens, M.H., Steele, A., Fogel, M.L., Bowden, R., Glamoclija, M., Zhang, Z., and Elardo, S.M. (2013) Unique Meteorite from Early Amazonian Mars: Water-Rich Basaltic Breccia Northwest Africa 7034. Science, 339, 780-785.

Basaltic Volcanism Study Project (1981) Basaltic volcanism on the terrestrial planets. Pergamon Press, Inc., 1286 pp.

Bell, A.S., Burger, P.V., Le, L., Shearer, C.K., Papike, J.J., Sutton, S.R., Newville, M., and Jones, J. (2014) XANES measurements of Cr valence in olivine and their applications to planetary basalts. American Mineralogist, 99, 1404-1412.

Berry, A.J., O'Neill, H.St.C., Scott, D.R., Foran, G.J. and Shelley, J.M.G. (2006). The effect of composition on Cr^{2+}/Cr^{3+} in silicate melts. American Mineralogist, 91, 1901-1908.

Borg, L.E. and Drake, M.J. (2005) A review of meteorite evidence for the timing of magmatism and of surface or near-surface liquid water on Mars. Journal of Geophysical Research, 110, E12SO3.

Borg, L.E., Nyquist, L.E., Wiesmann, H., Shih, C-Y. and Reese, Y. (2003) The age of Dar al Gani 476 and the differentiation history of the Martian meteorites inferred from their radiogenic isotopic systematics. Geochimica et Cosmochimica Acta, 67, 3519-3536.

Borg, L.E., Edmundson, J.E. and Asmerom, Y. (2005) Constraints on the U-Pb isotopic systematics of Mars inferred from a combined U-Pb, Rb-Sr and Sm-Nd isotopic study of the Martian meteorite Zagami. Geochimica et Cosmochimica Acta, 69, 5819-5830.

Borg, L.E., Symes, S., Marks, N., Gaffney, A., and Shearer, C.K. (2012) Constraints on the composition and evolution of the martian mantle from isotopic systematics of basaltic shergottites. In Workshop on the mantle of Mars: Insights from Theory, geophysics, high-pressure experiments, and meteorites, abstract 6014. Lunar and Planetary Institute, Houston.

Brandon, A.D., Puchtel, I.S., and Walker, R.J. (2012) How and when did the Mars mantle acquire its highly siderophile elements. In Workshop on the mantle of Mars: Insights from theory, geophysics, high-pressure experiments, and meteorites, abstract 6003. Lunar and Planetary Institute, Houston.

Canil, D. (2002) Vanadium in peridotites, mantle redox states and mantle environments: Archean to present. Earth and Planetary Science Letters, 195, 75-90.

Droop, G.T.R. (1987) A general equation for estimating Fe^{3+} concentrations in ferromagnesian silicates and oxides from microprobe analyses, using stoichiometric criteria. Mineralogical Magazine, 51, 431–435.

Elardo, S.M., Shearer, C.K. Jr., Fagan, A.L., Borg, L.E., Gaffney, A.M., Burger, P.V., Neal, C.R., Fernandes, V.A., and McCubbin, F.M. (2013) The origin of young mare basalts inferred from lunar meteorites Northwest Africa 4734, 032, and LaPaz Icefield 02205. Meteoritics & Planetary Science, 49, 261–291.

Fagan, T.J., Taylor, G.J., Keil, K., Bunch, T.E., Wittke, J.H., Korotev, R.L., Jolliff, B.L., Gillis, J.J., Haskin, L.A., Jarosewich, E., Clayton, R.N., Mayeda, T.K., Fernandes, V.A., Burgess, R., Turner, G., Eugster, O., and Lorenzetti, S. (2002) Northwest Africa 032: Product of lunar volcanism. Meteoritics & Planetary Science 37, 371–394.

Goodrich, C.A., Herd, C.D.K., and Taylor, L.A. (2003) Spinels and oxygen fugacity in olivine-phyric and lherzolitic shergottites. Meteoritics & Planetary Science, 38, 1773-1792.

Gardner-Vandy, K.G., Lauretta, D.S., and McCoy, T.J. (2013) A petrologic, thermodynamic and experimental study of brachinites: Partial melt residues of an R chondrite-like precursor. Geochimica et Cosmochimica Acta, 122, 36-57.

Gross, J., Treiman, A.H., Filiberto, J. and Herd, C.D.K. (2011) Primitive olivine-phyric shergottite NWA 5789: Petrology, mineral chemistry and cooling history imply a magma similar to Yamato-980459. Meteoritics & Planetary Science, 46, 116-133.

Haggerty, S.E. (1972) Luna 16: An opauqe mineral study and a systematic examination of compositional variations of spinels from mare Fecunditatis. Earth and Planetary Science Letters, 13, 328-352.

Haggerty, S.E. (1976) Opaque mineral oxides in terrestrial igneous rocks. In D. Rumble, Ed., Oxide Minerals, 3, p. Hg-101 – Hg-300. Reviews in Mineralogy, Mineralogical Society of America, Chantilly, Virginia.

Hanson, B. and Jones, J.H. (1998). The systematics of Cr^{3+} and Cr^{2+} partitioning between olivine and liquid in the presence of spinel. American Mineralogist, 83, 669-684.

Herd, C.D.K. (2006) Insights into the redox history of the NWA 1068/1110 martian basalt from mineral equilibria and vanadium oxybarometry. American Mineralogist, 91, 1616–1627.

Hill, R. and Roeder, P. (1974) The crystallization of basaltic liquid as a function of oxygen fugacity. Journal of Geology, 82, 709-729.

Ishizawa, N., Tateishi, K., Oishi, S., and Kishimoto, S. (2014) Bond-length fluctuation in the orthorhombic 3 x 3 x 1 superstructure of $LiMn_2O_4$ spinel. American Mineralogist, 99, 1528-1536.

Jurewicz, A.J.G., Mittlefehldt, D.W., and Jones, J.H. (1995) Experimental partial melting of the St. Severin (LL) and Lost City (H) chondrites. Geochimica et Cosmochimica Acta, 59, 391-408.

Karner, J., Papike, J.J., and Shearer, C.K. (2003) Olivine from planetary basalts: Chemical signatures that indicate planetary parentage and those that record igneous setting and process. American Mineralogist, 88, 806-816.

Kress, V.C., Carmichael, I.S.E. (1991) The compressibility of silicate liquids containing Fe_2O_3 and the effect of composition, temperature, oxygen fugacity and pressure on their redox states. Contributions to Mineralogy and Petrology, 108, 82-92.

Lindsley, D.H. (1976) Experimental studies of oxide minerals. In D. Rumble, Ed., Oxide Minerals, 3, p. L-61 – L-88. Reviews in Mineralogy, Mineralogical Society of America, Chantilly, Virginia.

Lindsley, D.H. (1991) Oxide Minerals: Petrologic and magnetic significance. Reviews in Mineralogy, 25, 509 pp. Mineralogical Society of America, Chantilly, Virginia.

Mallmann, G. and O'Niell, H.St.C. (2009) The crystal/melt partitioning of V during mantle melting as a function of oxygen fugacity compared with some other elements (Al, P, Ca, Sc, Ti, Cr, Fe, Ga, Y, Zr and Nb). Journal of Petrology, 50, 1765-1794.

McKay, G.A., Le, L., Schwandt, C., Mikouchi, T. and Koizumi, E. (2004a) Redox state and petrogenesis of Martian basalts: Clues from experimental petrology. Antarctic Meteorites, XXVIII, 44-45, National Institute of Polar Research, Tokyo.

McKay, G.A., Le, L., Schwandt, C., Mikouchi, T., Koizumi, E. and Jones, J. (2004b) Yamato 980459: The most primitive shergottite? In Lunar and Planetary Science 35, abstract 2154. Lunar and Planetary Institute, Houston.

Muan, A., Hauck and Lofall, T. (1972) Equilibrium studies with a bearing on lunar rocks, Proceedings of the 3rd Lunar Science Conference, 3, 185-196.

Nyquist, L.E., Ikeda, Y., Shih, C.-Y, Reese, Y.D., Nakamura, N. and Takeda, H. (2006) Sm-Nd age and Nd- and Sr- isotopic evidence for the petrogenesis of Dhofar 378. Antarctic Meteorites, XXX, 59-60, National Institute of Polar Research, Tokyo.

Papike, J.J., Karner, J.M., and Shearer, C.K. (2004) Comparative planetary mineralogy: V/(Cr + Al) systematics in chromite as an indicator of relative oxygen fugacity. American Mineralogist, 89, 1557-1560.

Papike, J.J., Karner, J.M., and Shearer, C.K. (2005) Comparative planetary mineralogy: Valence state partitioning of Cr, Fe, Ti, and V among the crystallographic sites in olivine, pyroxene, and spinel from planetary basalts. American Mineralogist, 90, 277-290.

Papike, J.J., Burger, P.V., Bell, A.S., Le, L., Shearer, C.K., Sutton, S.R., Jones, J., and Newville, M. (2013) Developing vanadium valence state oxybarometers (spinel-melt, olivine-melt, spinel-olivine) and V/(Cr + Al) partitioning (spinel-melt) for martian olivine-phyric basalts. American Mineralogist, 98, 2193-2196.

Papike, J.J., Burger, P.V., Bell, A.S., Shearer, C.K., Le, L., Jones, J., and Provencio, P. (2014) Valence state partitioning of V between pyroxene and melt for martian melt compositions Y 9805459 and QUE 94201: The effect of pyroxene composition and crystal structure. American Mineralogist, 99, 1175-1178.

Peslier, A.H., Hnatyshin, D. Herd, C.D.K., Walton, E.L., Brandon, A.D., Lapen, T.J. and Shafer, J.T. (2010) Crystallization, melt inclusion, and redox history of a Martian meteorite: Olivine-phyric shergottite Larkman Nunatak 06319. Geochimica et Cosmochimica Acta, 74, 4543-4576.

Righter, K., Sutton, S.R., Newville, M., Le, L., Schwandt, C.S., Uchida, H., Lavina, B., and Downs, R.T. (2006) An experimental study of the oxidation state of vanadium in spinel and basaltic melt with implications for the origin of planetary basalt. American Mineralogist, 91, 1643-1656.

Rodgers, D.R., Arnott, R.J., Wold, A., and Goodenough, J.B. (1963) The preparation and properties of some vanadium spinels. Physics and Chemistry of Solids, 24, 347-360.

Shearer, C.K., Burger, P.V., Papike, J.J., Borg, L.E., Irving, A.J. and Herd, C.D.K. (2008) Petrogenetic linkages among Martian basalts: Implications based on trace element chemistry of olivine. Meteoritics & Planetary Science, 43, 1241–1258.

Shearer, C., Burger, P.V., Neal, C.R., Sharp, Z., Spivack-Birndorf, L., Borg, L.E., Fernandes, V.A., Papike, J.J., Karner, J., Wadhwa, M., Gaffney, A., Shafer, J., Geissman, J., Atudorei, N.-V., Herd, C., Weiss, B.P., King, P.L., Crowther, S.A., and Gilmour, J.D. (2010). Non-basaltic asteroidal magmatism during the earliest stages of solar system evolution. A view from Antarctic achondrites Graves Nunatak 06128 and 06129. Geochimica et Cosmochimica Acta, 74, 1172-1199.

Sutton, S.R., Karner, J., Papike, J., Delaney, J.S., Shearer, C., Newville, M., Eng, P., Rivers, M., and Dyar, M.D. (2005) Vanadium K edge XANES of synthetic and natural basaltic glasses and application to microscale oxygen barometry. Geochimica et Cosmochimica Acta, 69, 2333-2348.

Symes, S.J.K., Borg, L.E., Shearer, C.K. and Irving, A.J. (2008) The age of the martian meteorite Northwest Africa 1195 and the differentiation history of the shergottites. Geochimica et Cosmochimica Acta, 72, 1696–1710.

Usui, T., Jones, J., and Mittlefehldt (2014) A partial melting study of an H-chondrite composition with application to the unique achondrite Graves Nunataks 06128 and 06129. Meteoritics & Planetary Science. In review.

Wadhwa, M. (2001) Redox state of Mars' upper mantle and crust from Eu anomalies in shergottite pyroxenes. Science, 291, 1527–1530.

Wechsler, B.A., Lindsley, D.H., and Prewitt, C.T. (1984) Crystal structure and cation distribution in titanomagnetites ($Fe_{3-X}TiO_4$). American Mineralogist, 69, 754-770.

FIGURE CAPTIONS

Figure 1. Spinel structural diagrams. a. The normal spinel structure represents magnesiocoulsonite, $^{IV}Mg^{VI}V^{3+}{}_2O_4$ (see Papike et al. 2005 and references therein). b. The inverse spinel structure (magnetite $^{IV}Fe^{3+}\ ^{VI}(Fe^{2+}Fe^{3+})O_4$). c. The V-inverse synthetic spinel structure ($^{IV}Fe^{2+}\ ^{VI}(Fe^{2+}V^{4+})O_4$). The structures are color coded as follows: Light blue represents oxygen ligands in all structures. Magnesiocoulsonite has yellow representing both Mg^{2+}-containing

530 tetrahedra and spheres. Red represents V^{3+} and V^{4+} octahedra and spheres. Magnetite has purple
531 representing Fe^{3+} tetrahedra, octahedra, and spheres, and green representing Fe^{2+}. V-inverse has
532 green representing Fe (both ferrous and ferric) and red representing V^{4+}. As the structure
533 evolves, from (a) normal spinel/ magnesiocoulsonite to (b) magnetite and from (a) to (c), with
534 increasing oxygen fugacity, V^{3+} in normal spinel is replaced by V^{4+} in inverse spinel and by Fe^{2+}
535 and Fe^{3+} in magnetite (an inverse spinel).
536
537 Figure 2. a. Shows the variation of Fe_2O_3 in spinel (wt.%). b. Shows modeled Cr^{3+}/total Cr in
538 melt. Error bars represent the 1σ standard deviation. c. Shows V_2O_3 in spinel (wt. %). d. Shows
539 modeled Fe_2O_3 in the liquid (wt. %). The modeled Cr valence in the melt was produced with the
540 data and methods described in Bell et al. (2014). The ferric/ferrous ratios of the melts were
541 modeled using the Kress and Carmichael (1991) equation and the EPMA determined melt
542 composition.
543
544 Figure 3. a. $D_V^{spinel/melt}$ (partition coefficient). Error bars represent the 1σ propagated error. b.
545 Measured $D_V^{spinel/melt}$, as in Figure 3a., with modeled partitioning curve overlain.
546
547 Figure 4. Spinel components chromite, magnetite, and other normal spinel, as a function of fO_2.
548
549 Figure 5. A cartoon that illustrates the combined effects of vanadium valence in the melt and the
550 increase in the magnetite component of the spinel.

Table 1. Experimental average values. Standard deviation (1σ) shown in parantheses.

$fO_{2:}$	IW-1		IW		IW+1		IW+2.2		FMQ		FMQ+1		FMQ+2	
Sample ID:	Y98C-21		Y98C-15		Y98C-10		Y98C-40		Y98C-19		Y98C-29		Y98C-31	
Oxide (Wt.%)														
SiO_2	0.26	(0.03)	0.18	(0.02)	0.26	(0.03)	0.16	(0.03)	0.15	(0.02)	0.17	(0.03)	0.17	(0.03)
Al_2O_3	8.62	(1.94)	8.40	(1.12)	8.14	(0.78)	6.74	(0.21)	5.96	(0.12)	7.30	(0.05)	6.95	(0.11)
Fe_2O_3*	0.94	(0.25)	2.35	(0.24)	3.59	(0.41)	6.30	(0.33)	8.12	(0.25)	17.27	(0.29)	17.53	(0.39)
TiO_2	2.79	(0.21)	2.37	(0.25)	2.04	(0.05)	1.42	(0.14)	0.90	(0.04)	1.89	(0.02)	1.72	(0.07)
Cr_2O_3	46.06	(1.94)	48.43	(1.74)	49.08	(1.81)	51.68	(0.63)	54.87	(0.42)	39.83	(0.11)	40.42	(0.76)
MgO	6.76	(0.24)	6.67	(0.21)	6.97	(0.18)	6.66	(0.11)	9.44	(0.08)	7.45	(0.04)	7.39	(0.07)
FeO	25.64	(0.31)	25.26	(0.25)	24.50	(0.23)	23.82	(0.12)	19.17	(0.13)	22.79	(0.06)	22.65	(0.19)
MnO	0.60	(0.02)	0.57	(0.01)	0.58	(0.01)	0.60	(0.02)	0.53	(0.02)	0.60	(0.02)	0.62	(0.02)
V_2O_3	9.16	(0.44)	6.56	(0.40)	5.58	(0.23)	2.80	(0.53)	1.58	(0.05)	2.40	(0.01)	2.22	(0.07)
Total	100.83		100.78		100.74		100.19		100.72		99.69		99.67	
A.F.U.														
Si	0.01	(0.00)	0.01	(0.00)	0.01	(0.00)	0.01	(0.00)	0.01	(0.00)	0.01	(0.00)	0.01	(0.00)
Al	0.34	(0.07)	0.33	(0.04)	0.32	(0.03)	0.27	(0.01)	0.24	(0.00)	0.30	(0.00)	0.28	(0.01)
Fe^{3+}*	0.02	(0.01)	0.06	(0.01)	0.09	(0.01)	0.16	(0.01)	0.21	(0.01)	0.45	(0.01)	0.45	(0.01)
Ti	0.07	(0.01)	0.06	(0.01)	0.05	(0.00)	0.04	(0.00)	0.02	(0.00)	0.05	(0.00)	0.04	(0.00)
Cr	1.23	(0.06)	1.29	(0.05)	1.31	(0.05)	1.40	(0.02)	1.46	(0.01)	1.08	(0.00)	1.10	(0.02)
Mg	0.34	(0.01)	0.34	(0.01)	0.35	(0.01)	0.34	(0.01)	0.47	(0.00)	0.38	(0.00)	0.38	(0.00)
Fe^{2+}	0.72	(0.01)	0.71	(0.01)	0.69	(0.01)	0.68	(0.00)	0.54	(0.00)	0.66	(0.00)	0.65	(0.00)
Mn	0.02	(0.00)	0.02	(0.00)	0.02	(0.00)	0.02	(0.00)	0.02	(0.00)	0.02	(0.00)	0.02	(0.00)
V	0.25	(0.01)	0.18	(0.01)	0.15	(0.01)	0.08	(0.01)	0.04	(0.00)	0.07	(0.00)	0.06	(0.00)
Total	3.00		3.00		3.00		3.00		3.00		3.00		3.00	
Components (Mol.%)														
Chromite	0.77		0.77		0.76		0.76		0.77		0.59		0.60	
Spinel	0.21		0.20		0.19		0.15		0.12		0.16		0.15	
Magnetite	0.01		0.04		0.05		0.09		0.11		0.24		0.25	
Glass (Wt.%)														
Cr_2O_3	0.37	(0.02)	0.22	(0.03)	0.20	(0.02)	0.13	(0.02)	0.13	(0.04)	0.12	(0.02)	0.12	(0.02)
V_2O_3	0.20	(0.02)	0.18	(0.02)	0.21	(0.01)	0.23	(0.02)	0.26	(0.03)	0.32	(0.02)	0.33	(0.02)
Partition Coefficient														
$D_V^{spinel/melt}$	45.19		36.75		26.52		12.37		6.19		7.55		6.77	

*Estimated using the methodology of Droop (1987).

Figure 1.

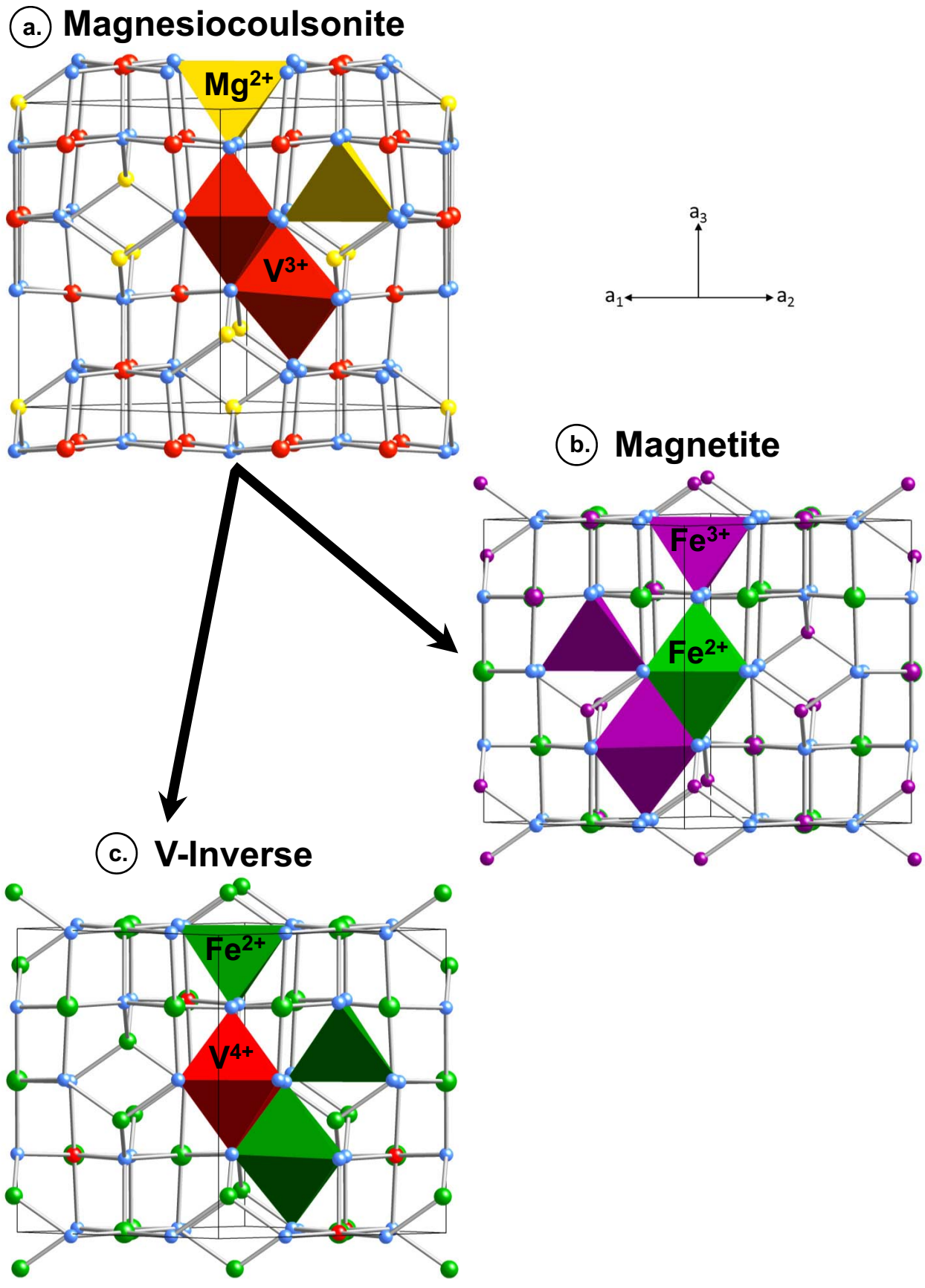
a. Magnesiocoulsonite
Mg2+
V3+
a3
a1
a2
b. Magnetite
Fe3+
Fe2+
c. V-Inverse
Fe2+
V4+

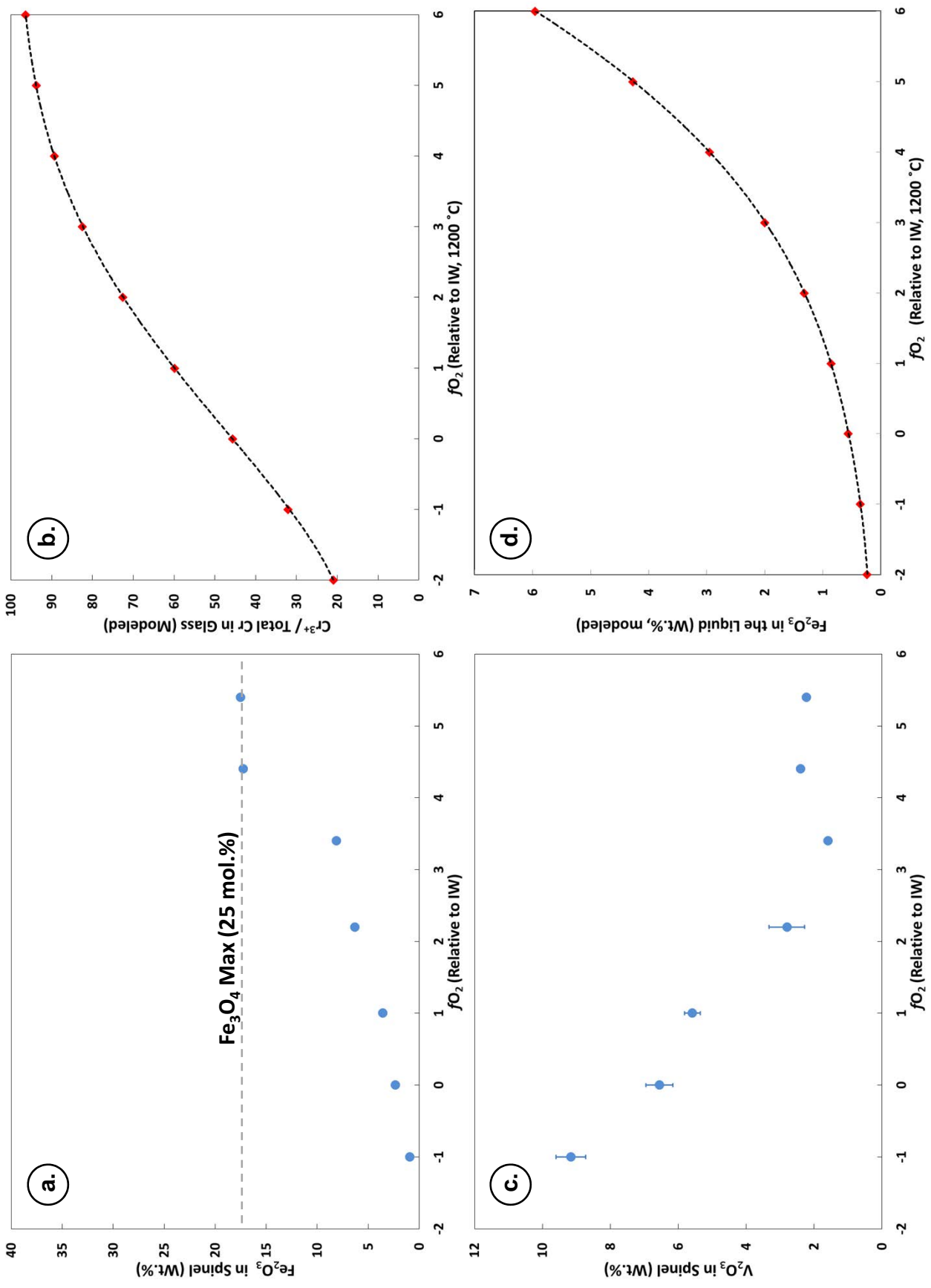
a.
Fe_3O_4 Max (25 mol.%)
Fe_2O_3 in Spinel (Wt.%)
fO_2 (Relative to IW)
b.
Cr^{3+} / Total Cr in Glass (Modeled)
fO_2 (Relative to IW, 1200 °C)
c.
V_2O_3 in Spinel (Wt.%)
fO_2 (Relative to IW)
d.
Fe_2O_3 in the Liquid (Wt.%, modeled)
fO_2 (Relative to IW, 1200 °C)

Figure 2.

Figure 3.

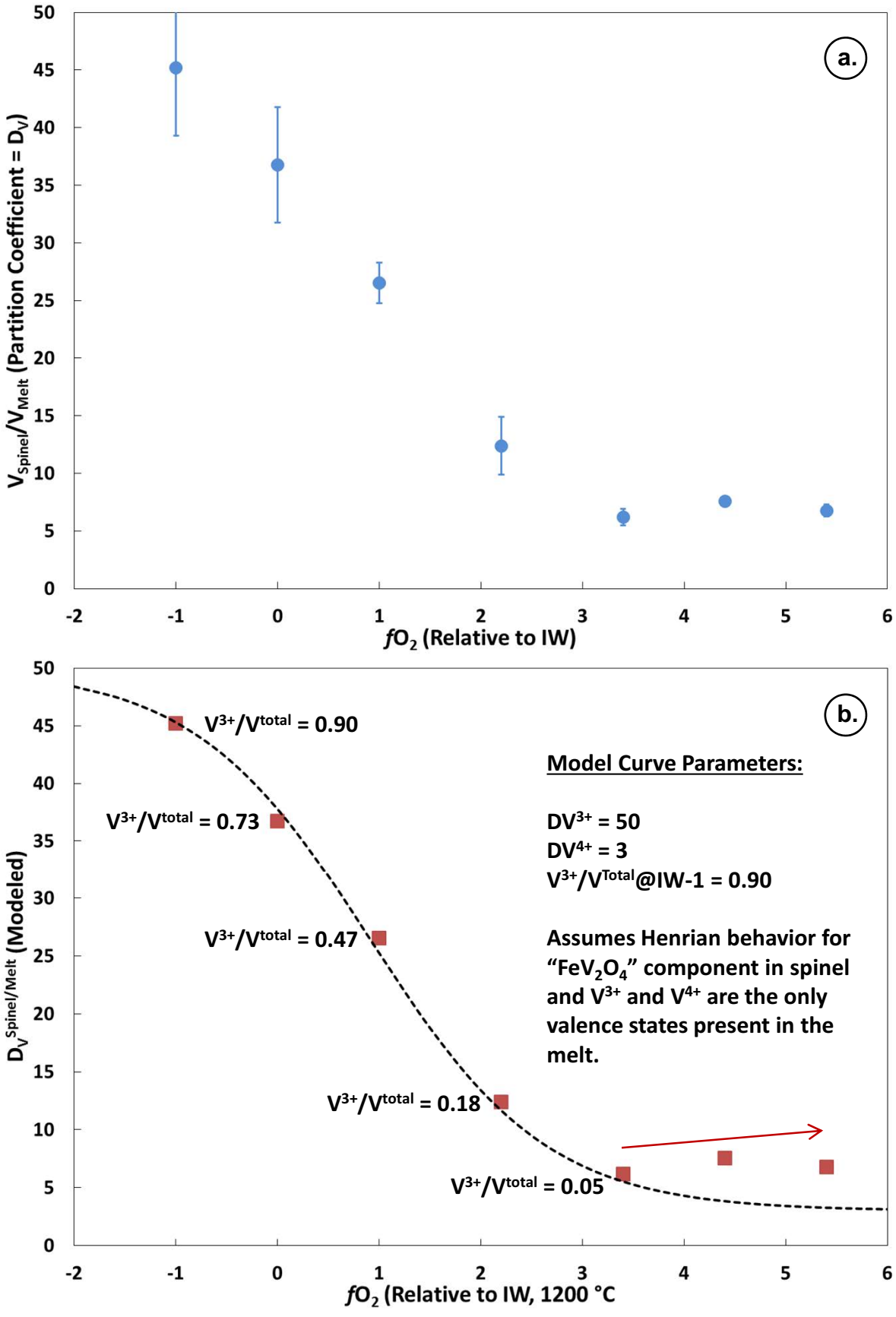
a.
V_{Spinel}/V_{Melt} (Partition Coefficient = D_V)
fO_2 (Relative to IW)
b.
$D_V^{Spinel/Melt}$ (Modeled)
V^{3+}/V^{total} = 0.90
V^{3+}/V^{total} = 0.73
V^{3+}/V^{total} = 0.47
V^{3+}/V^{total} = 0.18
V^{3+}/V^{total} = 0.05
Model Curve Parameters:
DV^{3+} = 50
DV^{4+} = 3
V^{3+}/V^{Total}@IW-1 = 0.90
Assumes Henrian behavior for "FeV_2O_4" component in spinel and V^{3+} and V^{4+} are the only valence states present in the melt.
fO_2 (Relative to IW, 1200 °C

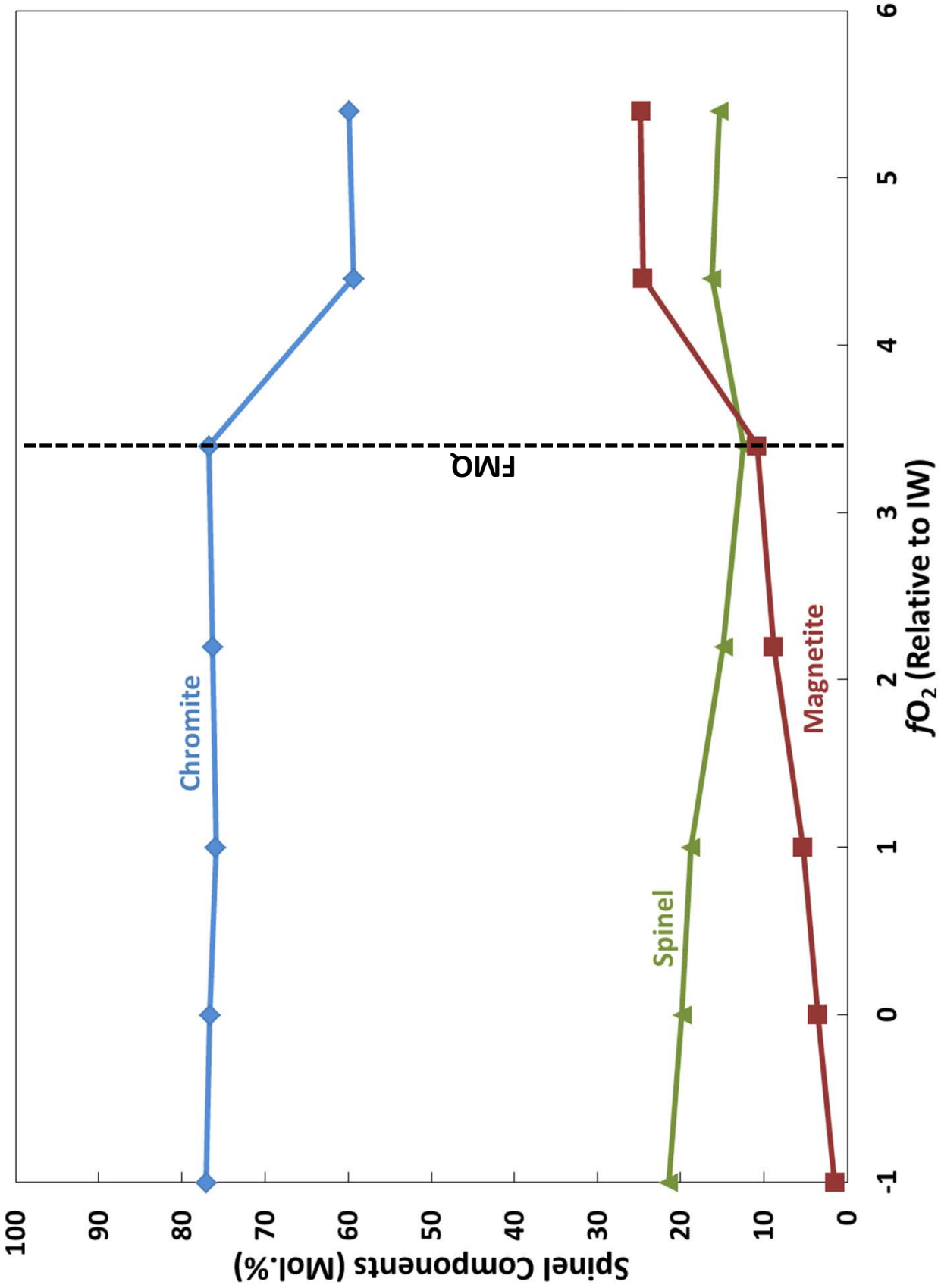
Spinel Components (Mol.%)
100
90
80
70
60
50
40
30
20
10
0
-1
0
1
2
3
4
5
6
fO_2 (Relative to IW)
FMQ
Chromite
Magnetite
Spinel

Figure 4.

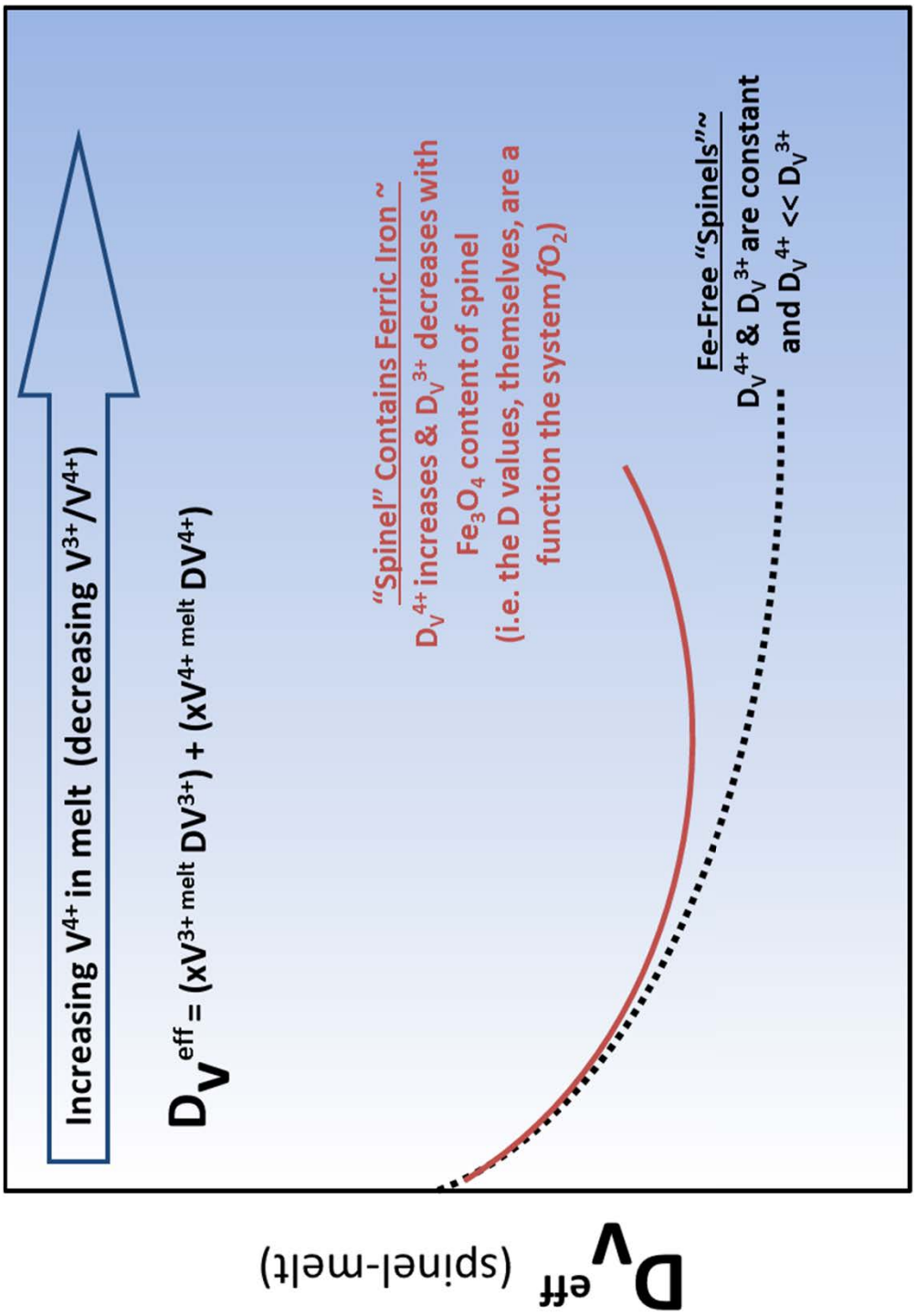
Increasing V^{4+} in melt (decreasing V^{3+}/V^{4+})
$D_V^{eff} = (xV^{3+\ melt}\ DV^{3+}) + (xV^{4+\ melt}\ DV^{4+})$
"Spinel" Contains Ferric Iron ~
D_V^{4+} increases & D_V^{3+} decreases with Fe_3O_4 content of spinel
(i.e. the D values, themselves, are a function the system fO_2)
Fe-Free "Spinels"~
D_V^{4+} & D_V^{3+} are constant
and $D_V^{4+} << D_V^{3+}$
D_V^{eff} (spinel-melt)
log fO_2

Figure 5.